

X-RAY POINT SOURCES IN THE SOMBRERO GALAXY: SUPERSOFT SOURCES, THE GLOBULAR CLUSTER/LMXB CONNECTION, AND AN OVERVIEW

R. DI STEFANO^{1,2}, A.K.H. KONG¹, M.L. VANDALFSEN^{3,4}, W.E. HARRIS³, S.S. MURRAY¹,
KISHA M. DELAIN⁵
Draft version October 18, 2018

ABSTRACT

We report on the population of point sources discovered during an 18.5 ksec *Chandra* ACIS-S observation of the Sombrero Galaxy. We present the luminosity function, the spectra of the 6 brightest sources, consider correlations with globular clusters (GCs) and with planetary nebulae (PNe), and study the galaxy's population of SSSs. We detected 122 sources, 22 of them are identified as luminous supersoft X-ray sources (SSSs). There is an over density of SSSs within 1.5 kpc of the nucleus, which is itself the brightest X-ray source. SSSs are also found in the disk and halo, with one SSS in a globular cluster (GC). This source is somewhat harder than most SSSs; the energy distribution of its photons is consistent with what is expected from an accreting intermediate mass black hole. Several sources in Sombrero's halo are good candidates for SSS models in which the accretor is a nuclear-burning white dwarf. In total, 32 X-ray sources are associated with GCs. The majority of sources with luminosity $> 10^{38}$ erg s⁻¹ are in GCs. These results for M104, an Sa galaxy, are similar to what has been found for elliptical galaxies and for the late-type spiral M31. We find that those optically bright GCs with X-ray sources house only the brightest X-ray sources. We find that, in common with other galaxies, there appears to be a positive connection between young (metal-rich) GCs and X-ray sources, but that the brightest X-ray sources are equally likely to be in metal-poor GCs. The luminosity function of X-ray sources in GCs has a cut-off near the Eddington luminosity for a $1.4M_{\odot}$ object. We propose a model which can explain the trends seen in the data sets from the Sombrero and other galaxies. Thermal-time scale mass transfer can occur in some of the the younger clusters in which the turn-off mass is slightly greater than $0.8M_{\odot}$; multiplicity may play a role in some of the most massive clusters; accretion from giant stars may be the dominant mechanism in some older, less massive and less centrally concentrated clusters. Key elements of the model can be tested.

Subject headings: galaxies: individual (M104) — X-rays: binaries — X-rays: galaxies

1. INTRODUCTION

M104 (NGC 4594), the Sombrero galaxy, is one of the most remarkable sights in the sky. Beyond its aesthetic appeal, the fact that it is a bright Sa galaxy which we view nearly edge on, provides insight into the organization of matter within spiral galaxies, allowing us to identify objects located out of the plane of the disk. During its second year of operations, *Chandra* conducted an 18.5 ksec observation of M104. We report here on the X-ray point sources discovered during this observation.

The results are remarkable because, in this relatively short observation of a galaxy located 8.9 Mpc from us (Ford et al. 1996), *Chandra* detected 122 point X-ray sources, 22 of them identified as very soft by an algorithm (Di Stefano & Kong 2003a, b) developed to search for luminous supersoft X-ray sources (SSSs). These observations provide the first glimpse of SSSs located a measurable distance away from the plane of the galaxy in which they reside.

M104 is estimated to contain ~ 1100 GCs, and therefore provides a good opportunity to study the relationship between X-ray sources and GCs. Thirty two of X-ray sources, including 1 SSS, are apparently associated with globular clusters (GCs). In fact, M104 is the first spiral outside the Local Group in which the connection between GCs and X-ray sources is being stud-

ied.

M104 is a LINER galaxy, and it has been conjectured that it houses an active galactic nucleus, making the nuclear region a prime target for X-ray observations. *ROSAT* High-Resolution Image observations identified 8 point-like sources, including one coincident with the nucleus, tentatively interpreted as a low-luminosity active galactic nucleus (AGN; Fabbiano & Juda 1997). *Beppo SAX* observations, coupled with a short (1.7 ksec) *Chandra* exposure also support the AGN model, although a superposition of sources in the nuclear region could not be ruled out (Pellegrini et al. 2002). The diffuse emission is also being studied (Forman et al. 2003; see Delain et al. 2001, which also includes a preliminary analysis of the point sources).

The focus of this paper is on the rich point source population revealed by the unique angular resolution of *Chandra*. In §2 we discuss the observations and data reduction, focusing in §3 on an overview of the source properties: IDs with GCs and planetary nebulae, the spectra of the nuclear source and of the 6 brightest non-nuclear sources, the luminosity function, and color-color diagram. Our main science results are on SSSs, discussed in §4, and on the connection between GCs and low-mass X-ray binaries (LMXBs), discussed in §5. §6 highlights our conclusions and discusses prospects for future observations.

¹ Harvard-Smithsonian Center for Astrophysics, 60 Garden Street, Cambridge, MA 02138; rd@cfa.harvard.edu

² Department of Physics and Astronomy, Tufts University, Medford, MA 02155

³ Department of Physics and Astronomy, McMaster University, 1280 Main Street W, Hamilton, ON, L8S 4M1, Canada

⁴ Visiting astronomer, Canada-France-Hawaii Telescope, operated by the National Research Council of Canada, the Centre National de la Recherche Scientifique de France, and the University of Hawaii

⁵ University of Minnesota, Department of Astronomy, Minneapolis, MN 55455

2. OBSERVATIONS AND DATA REDUCTION

M104 was observed by *Chandra* on 31 May 2001 with the Advanced CCD Imaging Spectrometer (ACIS-S). The effective exposure time was about 18.5 ks. In this paper, we focus only on the data taken with the S3 CCD. The nuclear region of M104 was placed near the aim-point of the ACIS-S array. All data were telemetered in faint mode and were collected with a frame transfer time of 3.2 s. In order to reduce the instrumental background, only data with *ASCA* grades of 0, 2, 3, 4, and 6 were included. We ran the detection algorithm in the energy range 0.1–7 keV and visually inspected the regions around each source. We also inspected the background count rates from the S1 chip; no significant background flares were found. The data reduction and analysis was done with CIAO, Version 2.3 and energy spectra were analyzed with XSPEC, Version 11.2.

Discrete sources in the image were found with WAVDETECT (Freeman et al. 2002) together with an exposure map. A total of 122 sources were detected. Source count rates were determined via aperture photometry. The radius of the aperture was varied with average off-axis angle in order to match the 90% encircled energy function. Background was extracted from an annulus centered on each source. In some cases, for example, near the nucleus, we modified the extraction region to avoid nearby sources. It was also necessary to modify the extraction radius for some faint sources that are close to more luminous sources. Every extraction region was examined carefully in the image. The count rate was corrected for exposure, background variation, and instrumental PSF. All sources in the catalog have signal-to-noise ratio (S/N) > 2.6 and only 12 sources have S/N < 3 with the minimum number of counts equal to 7.

Table 1 lists the 122 sources in our catalog, sorted in order of increasing right ascension. The position of each detected source listed in Table 1 was corrected for astrometry with the Two Micron All Sky Survey (2MASS) catalog (Cutri et al. 2000). Within S3, we found six X-ray sources located within 1'' of 2MASS stars (see Table 1). We calculated the average coordinate shift for the six sources and used this to correct the *Chandra* position. The shift in R.A. and Dec. is 0.17'' and 0.25'', respectively. The average displacement between the X-ray and 2MASS positions after the shift is about 0.15''.

Some of the sources may be background active galactic nuclei (AGNs). We estimated the contribution of background unrelated objects by the *Chandra* Deep Field Surveys (e.g., Brandt et al. 2001; Giacconi et al. 2001). We found that at 4.5×10^{37} erg s⁻¹ (the completeness limit), fewer than 10 sources are likely to be background objects. We expect that only a small fraction of the ~ 10 background objects are soft enough to be identified as SSSs. To quantify this, we have studied data from several fields observed by *Chandra*⁶ and find that 1–3 SSSs unrelated to M104 are likely to be present in our data; these are most likely to be foreground stars (see e.g. Di Stefano et al. 2003). In fact, 2 foreground stars are identified as SSSs. For more details on how the analysis was conducted, see Di Stefano et al. 2001 and Kong et al. 2002.

3. PROPERTIES OF X-RAY SOURCES

3.1. Source Identification

Observations at optical wavelengths have identified globular clusters and planetary nebula in M104 (VanDalfsen et al. 2001; Larsen, Forbes, & Brodie 2001; Ford et al. 1996). We searched for coincidences between these catalogs and our *Chandra* sources. There are 640 GCs identified from the ground (VanDalfsen et al. 2001) in the field of view of S3. Moreover, 72 additional GCs were found by using *HST* (Larsen et al. 2001). It is worth noting that the astrometry of the *HST* image (Larsen et al. 2001) was not well calibrated and we therefore corrected the astrometry by using the 2MASS catalog in our analysis. In addition, we also checked the USNO-B1.0 (Monet et al. 2003) and 2MASS (Cutri et al. 2000) catalogs. We included all the coincidences in Table 1. Since the astrometry of these catalogs is better than 1'', we used a searching radius of 1.5'' to search for GCs and planetary nebula. We found 32 X-ray GCs (25 from the ground and 7 from *HST*) out of 742 optically identified GCs within S3, while we did not find X-ray emitting planetary nebula. The general properties of these X-ray GCs will be discussed in detail in next subsections. There are 3 (4) X-ray GCs that are also coincident with 2MASS (USNO) sources.

In order to estimate the accidental correlation rate, we shifted all the *Chandra* sources by 4'', 6'', 8'' and 10'' to the north, east, south, west, northeast, northwest, southeast, and southwest, and ran the search for each of the catalogs. The average accidental matching rates for GCs catalog from the ground, GCs catalog from the *HST* and PN catalog are 2.8, 3.9, and 0.7 respectively. We therefore estimate that 22 of the X-ray sources associated with GCs identified from ground-based observations and 3 from *HST* observations represent genuine matches. The relatively higher accidental matching rate for the *HST* catalog may due to the crowding in the nuclear region of M104. The analyses presented in the remainder of the paper apply to only the GCs observed from the ground.

3.2. The Nuclear Source

Pellegrini et al. (2002) used a 1.7 ksec ACIS-S observation to study the spectrum of the central source. They found a power-law fit ($\alpha = 1.5^{+0.4}_{-0.3}$), with $N_H = 1.7^{+1.1}_{-0.9} \times 10^{21}$ cm⁻². The flux was 1.6×10^{-12} erg cm⁻² s⁻¹, which translates to $L = 1.5 \times 10^{40}$ erg s⁻¹ at 8.9 Mpc. During the 18.5 ksec observation, photons from the nuclear source were piled up (~ 20%). By using a pile-up model developed for *Chandra* data (Davis 2001), we found a power-law fit ($\alpha = 2.18^{+0.35}_{-0.35}$), with $N_H = 2.9^{+0.57}_{-0.57} \times 10^{21}$ cm⁻²; assuming the distance of 8.9 Mpc, $L = 2.0 \times 10^{40}$ erg s⁻¹. The properties of the nuclear source in the second, longer observation we report on are roughly consistent with those described by Pellegrini et al. (2002). They are also consistent with an analysis including *XMM-Newton* data (see Pellegrini et al. 2003 for a more complete discussion of the nuclear source).

3.3. Spectral fits of bright sources

We extracted the energy spectra for the 6 brightest sources (> 100 counts), and fitted them to simple one-component spectral models including absorbed power-law, blackbody, disk blackbody, and Raymond-Smith models. The background spectrum was extracted from source-free regions around each source. We also corrected for the degradation of soft energy (< 1 keV) sensitivity⁷. Table 2 lists the spectral fits of these sources. Except

⁶ <http://hea-www.cfa.harvard.edu/CHAMP>

⁷ see http://asc.harvard.edu/ciao/threads/apply_acisabs/

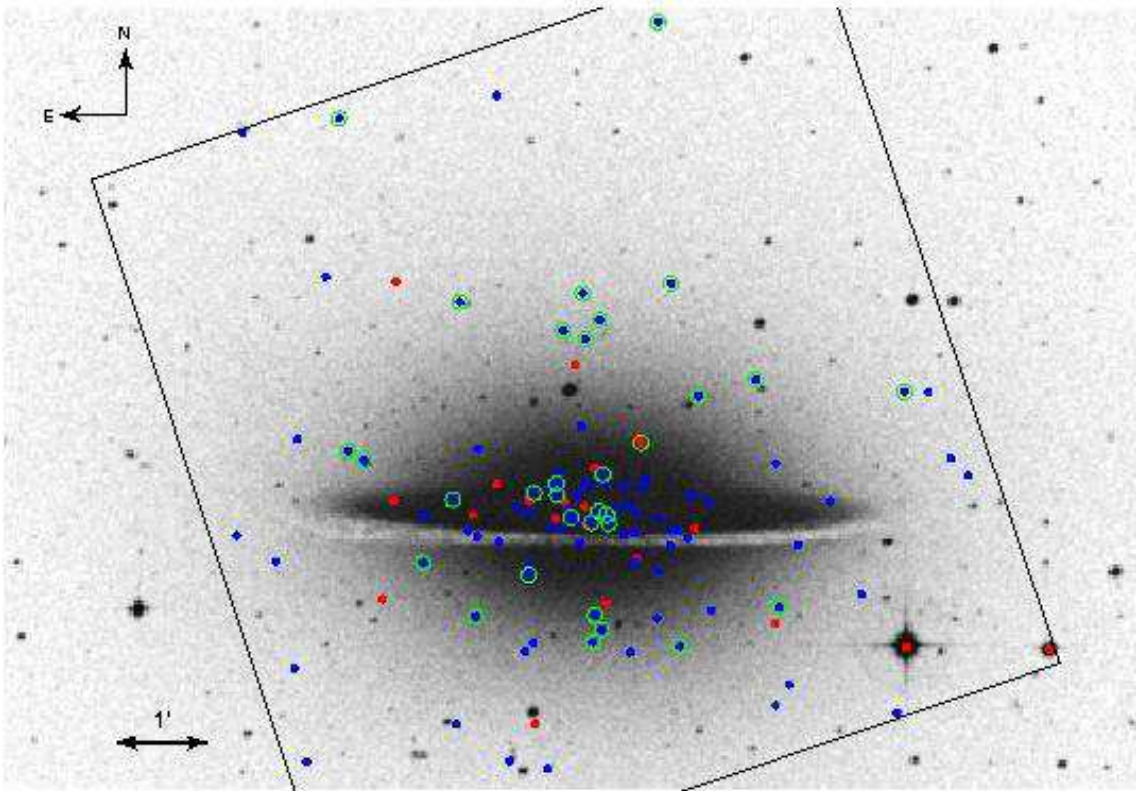


FIG. 1.— Detected X-ray sources (blue and red filled circles) overlaid on an optical Digital Sky Survey image of M104. SSSs are shown as red filled circles while X-ray GCs are marked with green open circles. To be identified as a match, a GC and an X-ray source must lie within $1.5''$ of each other; note, however, that to show the matches clearly, the green circles have a much larger radius ($5''$). The field of view of the S3 CCD is marked as a black line. North is up, and east is to the left.

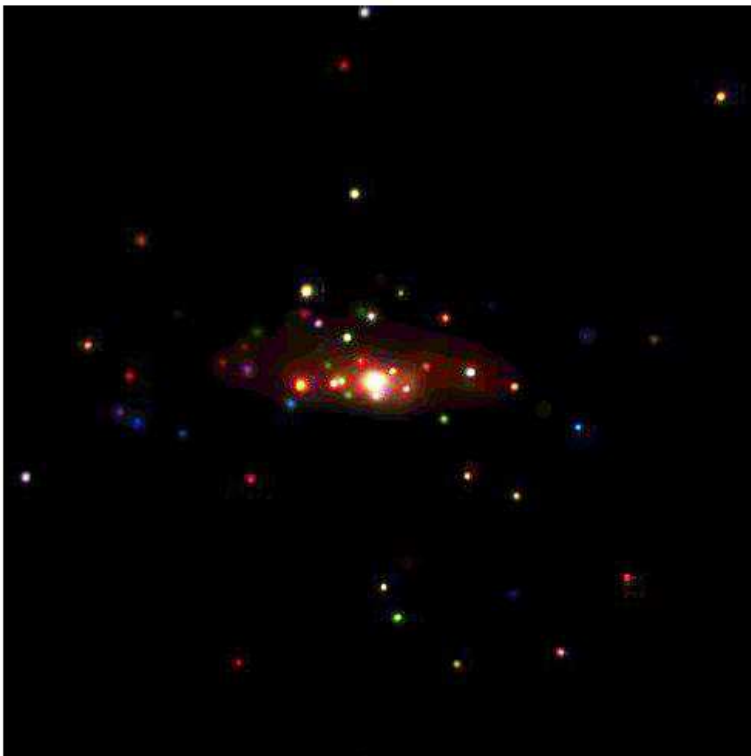


FIG. 2.— “True color” *Chandra* image of the central $4' \times 4'$ region of M104. The three energy bands are 0.1–1.1 keV (red), 1.1–2 keV (green), and 2–7 keV (blue). The image has been exposure corrected and adaptively smoothed. North is up, and east is to the left. Note the extended diffuse emission near the galaxy’s center. The background subtraction method we applied should minimize the influence of this diffuse emission on estimates of the broadband count rates of point sources; nevertheless, the uncertainty in the numbers of counts in each band (S, M, and H) is larger than it would otherwise be for those X-ray sources located in regions with significant amounts of diffuse emission.

for X5 which is a bright foreground star ($B = 10.3$), all sources can be fit with a single-component model. The spectral shape of X9, X38, X59, and X79 is consistent with an absorbed power-law model with photon index between 1.1 and 2. These spectra are similar to typical X-ray binaries seen in our own Galaxy and in other galaxies. Figure 3 shows the energy spectrum of the brightest point source (excluding the nucleus), X79. X82 is soft compared with the other sources; the energy spectrum is a blackbody model with thermal temperature of 0.18 keV (see Table 2 and Figure 3) and it is also classified as an SSS (see above). The foreground star, X5, is soft and requires a Raymond-Smith plus power-law model (see Table 2). The values of N_H are generally low and are roughly consistent with the Galactic value along the direction to M104 ($N_H = 3.7 \times 10^{20} \text{ cm}^{-2}$). The 0.3–7 keV luminosities of these sources (excluding X5) range from $4 \times 10^{38} \text{ erg s}^{-1}$ to $1 \times 10^{39} \text{ erg s}^{-1}$ at a distance of 8.9 Mpc.

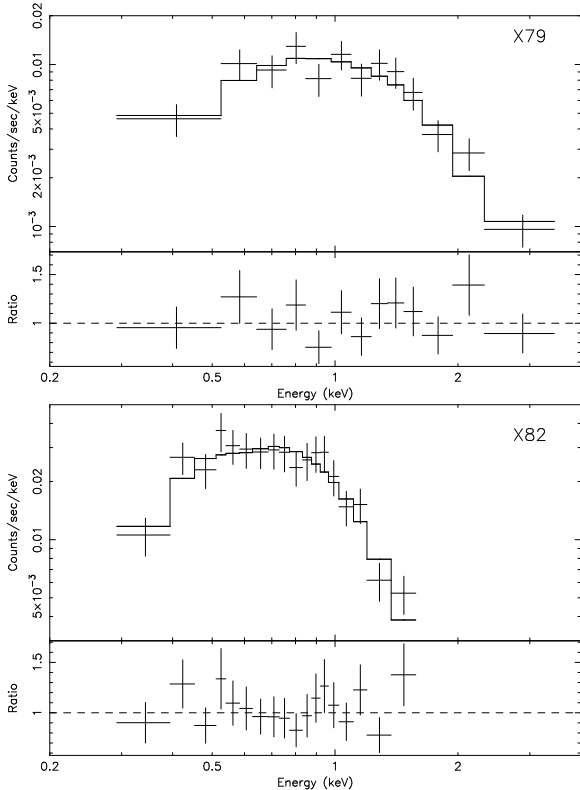


FIG. 3.— Spectral fit to X79 (power-law model with $N_H = 1.1 \times 10^{21} \text{ cm}^{-2}$ and $\alpha = 2.04$), and X82 (blackbody model with $N_H = 0.85 \times 10^{20} \text{ cm}^{-2}$ and $kT = 0.18 \text{ keV}$).

3.4. X-ray Luminosity Function

We constructed the X-ray point source luminosity function (LF). The count rates for all detected sources were converted into unabsorbed 0.3–7 keV luminosities by assuming an appropriate spectral model. For the brightest 6 sources (Table 2), we used the luminosities derived from the best-fitting spectral model. In addition, we excluded all the foreground stars (see Table 1). In Figure 4, we plot the cumulative luminosity functions for all sources (excluding GCs) and X-ray GCs. Because we have eliminated foreground stars and expect that fewer than 10 of the X-ray sources are background AGN (see §2), these luminosity functions should primarily describe the properties of sources associated with M104.

To estimate the completeness limit, we used similar method by Kong et al. (2002, 2003a). We computed histograms of the number of detected sources against the S/N to examine the completeness limit; the histograms peak at $S/N \sim 3.2$, corresponding to $4.5 \times 10^{37} \text{ erg s}^{-1}$, and fall off below this. Hence the luminosity function is complete down to $4.5 \times 10^{37} \text{ erg s}^{-1}$. It is clear that the two luminosity functions are not well-described by a simple power-law. Instead, they both have a break or cutoff at near $1 - 3 \times 10^{38} \text{ erg s}^{-1}$. In addition, power-law models may not be good descriptions above and/or below the breaks. We nevertheless use a broken power-law model for each LF, to facilitate comparison with other treatments (see, e.g., Sarazin et al. 2001). The function is defined as:

$$\frac{dN}{dL_{38}} = A \left(\frac{L_{38}}{L_b} \right)^{-\Gamma} \quad (1)$$

where $\Gamma = \Gamma_1$ for $L_{38} \leq L_b$, $\Gamma = \Gamma_2$ for $L_{38} > L_b$, and L_{38} is the 0.3–7 keV X-ray luminosity in units of $10^{38} \text{ erg s}^{-1}$. We used a maximum likelihood method (e.g., Crawford, Jauncey, & Murdoch 1970) to fit the differential luminosity functions of point sources (excluding nucleus, GCs, and stars) and X-ray GCs with a broken power law. For X-ray point sources, the luminosity break is at $9_{-1.6}^{+2.0} \times 10^{37} \text{ erg s}^{-1}$, while $\Gamma_1 = 0.74_{-1.04}^{+0.84}$, $\Gamma_2 = 2.58_{-0.28}^{+0.35}$, and $A = 45.85$. For X-ray GCs, the shape is nearly a cutoff power law with a luminosity break at $3.1_{-0.24}^{+0.26} \times 10^{38} \text{ erg s}^{-1}$, $\Gamma_1 = 0.67_{-0.39}^{+0.36}$, $\Gamma_2 = 8.6_{-3.2}^{+4.6}$, and $A = 5.90$.

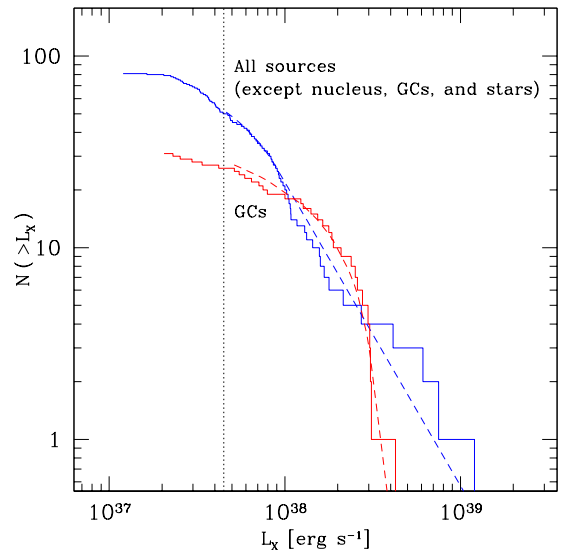


FIG. 4.— Cumulative luminosity functions and their best-fit model of X-ray point sources (blue; excluding the nucleus and stars) and GCs (red) in M104. The vertical dotted line represents the completeness limit ($4.5 \times 10^{37} \text{ erg s}^{-1}$) of our data.

3.5. Color-color Diagram

Many of the detected sources provide fewer than 100 counts, which makes it difficult to derive spectral parameters. However, hardness ratios can give a crude indication of the X-ray spectra. We therefore computed the hardness ratios for each detected sources, for which we define $HR1 = (\text{medium-soft}) / (\text{medium+soft})$ and $HR2 = (\text{hard-soft}) / (\text{hard+soft})$ to plot the color-color diagram as shown in Figure 4. We calculated the 1σ uncertainties of the hardness ratios by using a maximum likelihood method as used in the *Einstein* catalog (Harris et al. 1993).

4. SUPERSOFT X-RAY SOURCES

SSSs have luminosities in the range $10^{35} - 10^{39}$ erg s $^{-1}$. and kT in the range 10–100 eV. SSSs in our Galaxy are largely obscured from us by the interstellar medium (ISM); it is therefore possible that this poorly understood class is in fact the dominant class of high luminosity X-ray binaries. Di Stefano & Rappaport (1994) estimated, based on *ROSAT* observations and simple models of galaxy absorption, that the Milky Way and M31 may each harbor on the order of 1000 SSSs with $L_X > 10^{37}$ erg s $^{-1}$ and $kT > 30$ eV. SSSs may significantly influence their galactic environments, both as efficient ionizers of the interstellar medium and possibly also as progenitors of Type Ia supernovae.

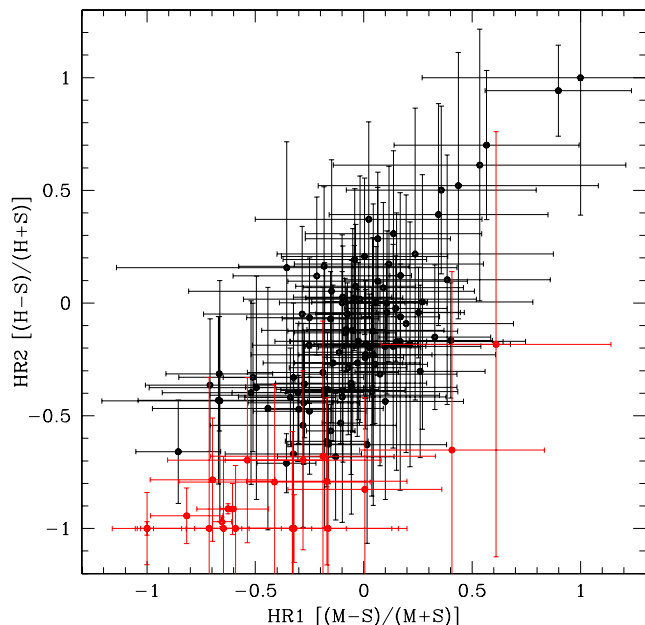


FIG. 5.— Color-color diagram of all X-ray point sources in M104. SSSs are marked with red lines.

Some SSSs are simply hot WDs (e.g., post novae), pre-white-dwarfs (in planetary nebulae), or symbiotics. However, the physical nature of a majority of the SSSs with optical IDs is not yet understood. These more mysterious sources include CAL 83 and CAL 87 (Long, Helfand, & Grabelsky 1981), as well as 7 sources discovered with *ROSAT* (see Greiner 2000 for details). Black hole (BH; Cowley et al. 1990) and accreting-neutron-star models (Greiner et al. 1991, Kylafis & Xilouris 1993) may apply to some SSSs. Binary models which predict quasi-steady nuclear burning of accreted matter on the surface of a WD are considered promising (see, e.g., van den Heuvel et al. 1992.) Nevertheless, studies of external galaxies find some SSSs that may be BHs with $M \sim 100M_{\odot}$ (Di Stefano & Kong 2003a, Kong & Di Stefano 2003).

The primary goals we hope to achieve by conducting SSS searches in external galaxies are to gain an understanding of the physical nature or natures of the sources and to eventually improve estimates of the sizes of galaxy populations of SSSs. We gain important insight by being able to study the locations of SSSs relative to large-scale galaxy structures (bulge, disk, halo), to study the stellar populations within which SSSs are embedded, to establish luminosity distributions, and spectral characteristics for large samples of sources, and to estimate total populations as a function of galaxy properties. A challenge

that must be met by any such program of study is that the small number of counts we receive from X-ray sources in external galaxies makes spectral classification difficult. Selection is further complicated by the fact that we have only a small sample of local (Galaxy and Magellanic Cloud) sources, whose properties may not span the full range of SSS properties. Di Stefano & Kong (2003a, b) have developed an algorithm to select SSSs in external galaxies. Its application has led to some intriguing results.

In M101, SSSs appear to be primarily associated with the spiral arms; this, combined with the locations of several SSSs near HII regions and/or OB associations, suggests that some SSSs are relatively young systems. In M31 (but not in M101), there is a bright bulge population of SSSs, including one source within a few parsecs of the nucleus. This suggests that some SSSs within ~ 1 kpc of a massive BH may be the stripped cores of giants that have been tidally disrupted by the BH (Di Stefano et al. 2001). Several galaxies house ultraluminous SSSs (with $L_X > 10^{39}$ erg s $^{-1}$) that may be accreting intermediate-mass ($\sim 50 - 10^4 M_{\odot}$) BHs. These BH spectra typically include some photons with energies above 1.1 keV, even though 90% of the flux is carried by photons of lower energy. Elliptical galaxies (e.g., NGC 4697 (Sarazin et al. 2001)) contain SSSs, including SSSs in GCs (NGC 4472 (Friedman et al. 2002)).

We applied our algorithm to the X-ray sources we identified in M104. In Table 1, SSSs marked either “HR” or “ $3-\sigma$ ” are likely to have spectra similar to those of the SSSs studied so far the the Magellanic Clouds and Milky Way. Sources labeled “med” or “noh”, may be highly absorbed, or may have somewhat higher temperatures, but kT is still smaller than approximately 250 eV. Sources marked “ σ ”, “ $3\sigma 1$ ” or “HR1” could have temperatures in the same general range as “med” or “noh” SSSs; our studies of SSSs in other galaxies show, however, that some have spectra as soft as the “HR” or “ 3σ ” sources, but also include a small ($< 10\%$) harder component.

Roughly one in six X-ray sources in M104 satisfies the conditions designed to identify SSSs. Below we discuss the luminosity distribution of the SSSs detected in M104, and an intermediate-mass BH model for the brightest SSS in M104. The unique feature of M104, is that one can identify and study the disk, bulge, and halo populations of SSSs; these are discussed in §4.3-§4.5.

4.1. Luminosity Distribution of SSSs

The dimmest GC X-ray source (2×10^{37} erg s $^{-1}$) and the 6 dimmest non-GC X-ray sources (starting at 1.4×10^{37} erg s $^{-1}$) are all SSSs. In fact, of 82 non-GC X-ray sources, 15 of the 30 least luminous, are SSSs; these represent 3/4 of the non-stellar SSSs. The dim SSSs each provide 8–20 photons.

We expect low-count-rate SSSs for two reasons. First, the intrinsic SSS luminosity function of some SSSs is dominated by low-L sources. The luminosity of nuclear-burning WDs, e.g., increases with increasing WD mass, with L nearing the Eddington limit and kT perhaps in excess of 100 eV, as the WD mass approaches the Chandrasekhar mass. Since, however, WDs with lower mass are more common, most nuclear-burning WDs should be less luminous. In addition, Greiner et al. (1999) and Greiner & Di Stefano 1999, established that there is a lower-luminosity extension of the class of SSSs, which presumably corresponds to nuclear-burning WDs of even lower mass than those in the systems first observed with *Einstein* and *ROSAT*. The number of systems in our Galaxy capable of ap-

pearing as such lower-luminosity SSSs may be approximately 10,000. Second, the effects of absorption on the radiation emitted by SSSs is severe. The 18.5 ksec observation of M104 was likely to only detect those SSSs on the outer edge of the side of the disk and bulge nearest to us.

In spite of the numerical dominance of the low count rate SSSs, SSSs are also well represented among the most luminous SSSs. Three of the 12 brightest M104 X-ray sources are SSSs—these include one of the brightest non-nuclear sources, X82.

4.2. Intermediate-Mass BH Model for the Brightest SSS

X82 is an SSS located in the bulge of M104. The spectral fit is shown in Figure 3. The spectral parameters (Table 2) are: $kT = 180$ eV, $L_X = 8.9 \times 10^{38}$ erg s⁻¹, $N_H = 0.9_{-0.9}^{+4.6} \times 10^{20}$ cm⁻². This fit cannot provide a unique physical interpretation. It is, however, consistent with the model of an intermediate-mass BH. Consider a geometrically thin but optically thick accretion disk, and identify the inner edge of the disk with the last stable orbit around an accreting BH. If we assume an emission efficiency of 10% (i.e., that 10% of the rest energy of matter falling into the BH is radiated by the disk), then

$$M_{BH} = 10^3 M_\odot \left[\frac{49 \text{ eV}}{kT} \right]^2 \left[\frac{L}{2.9 \times 10^{37} \text{ erg/s}} \right]^{\frac{1}{2}} \quad (2)$$

For the spectral parameters derived in the fit, we find that the mass of the BH would be $\sim 400 M_\odot$. This is likely to be a lower limit, since spectral hardening effects, orientation effects, and spin would all tend to increase the derived value of the mass.

4.3. SSSs in the Bulge of M104

There is a clear over density of SSSs in the region near the nucleus: 4 SSSs are located within ~ 1 kpc of the galaxy center, and an additional 3 SSSs are located within 1.5 kpc of the center. Since this places 1/3 of the SSSs in roughly 2% of the area containing SSSs, it is clear that this overdensity implies that some of these 7 SSSs are physically close to the nucleus. In M31 there are SSSs within several parsecs of the nucleus, and members of the bulge population are among the most luminous SSSs in the galaxy. While it is possible that all or most of these sources are simply descended from the stellar populations that inhabit the bulge, the presence of SSS very close to the nucleus of M31 has suggested that some bulge SSSs may be the stripped cores of stars that have been tidally disrupted by a central BH. If this is so, then galaxies with massive BHs, such as M104, with an estimated BH mass of $10^9 M_\odot$, should have a central overdensity of SSS.

4.4. SSSs in the Disk of M104

Given the small numbers of SSSs observed near the disk, coupled with the large size of the bulge, it is difficult to definitely identify SSSs as members of a disk population. Indeed, SSSs in or near the disk are the ones most likely to be subject to absorption. The locations of X21 (9 counts), X37 (9 counts), X110 (15 counts), and possibly X102 (20 counts) are consistent with membership in the disk. Indeed the distributions of counts in S, M, and H for at least 3 of these sources (X37, X110, and X102) would be consistent with what is expected for a highly luminous, highly absorbed source with $kT \sim 100$ eV.

4.5. SSSs in the Halo of M104

One of the most exciting aspects of the M104 observations is that for the first time, we can unambiguously identify SSSs located out of the disk of a spiral galaxy. (See also Di Stefano et al. 2003a, on M31.) The 2 softest sources, X71, and X86, are each located > 4 kpc away (north and south, respectively) from the galactic disk. Neither is associated with a known GC or with any other optical counterpart on the DSS image. From neither source have we received photons with energies > 1.1 keV. The estimated luminosity of X71 is 1.4×10^{37} erg s⁻¹, while for X86 we derive 1.6×10^{38} erg s⁻¹. (These estimates use a model with $kT = 125$ eV and $N_H = 5 \times 10^{20}$ cm⁻².) If these are not foreground or background objects, they may be good candidates for the NBWD model. Since such systems should not have experienced prior supernova explosions, they are unlikely to have been ejected from the disk. They are therefore likely descendants of an old halo stellar population. A particularly interesting SSS is X35, which is in a GC. (From its position alone, it could be part of the bulge or halo.) This source does emit photons between 1.1 and 2 keV. The source properties are consistent with those of a BH accretor with mass equal to $\sim 50 M_\odot$ (See equation (2)). This is similar to the situation we have found in NGC 4472, where at least 5 SSSs are associated with GCs, several amenable to a similar interpretation (Friedman et al. 2002, Di Stefano et al. 2003b).

4.6. Relationship between SSSs and Planetary Nebulae

In the region covered by the S3 CCD, 249 PNe have been identified. None of these is near enough to an X-ray source to suggest a physical association. The fact that no PNe are associated with SSSs is interesting. Because SSSs emit highly ionizing radiation. Indeed, one SSS in the Magellanic Clouds is a PN (Wang 1991). SSSs that are binary systems can ionize the interstellar medium in which they are embedded. Those located in regions in which the ISM has a density greater than ~ 1 atom cm⁻³, can create circumstellar ionization nebulae with very large (radiation-limited) radii (> 10 pc) (Rappaport et al. 1994). CAL 83, located in the Magellanic Clouds is embedded in such a nebula (Remillard, Rappaport, & Macri 1995). With two of twelve Magellanic Cloud SSSs associated with nebulae, and with ~ 1000 SSSs predicted in galaxies such as M31, we might expect there to be dozens of such associations. The nebulae could be and would likely be included among PNe lists by surveys using the methodology Ford et al (1996) used to identify PNe in M104 (Di Stefano, Paerels, & Rappaport 1995). Because only a small fraction of all SSSs can be detected, the number of observable PN/SSS may be only 1–10% of the number of physical associations. We might expect some matches for M104 (Di Stefano, Paerels, & Rappaport 1995). The lack of any such associations may mean that SSSs are typically in regions that have a very low density ISM, or that they typically are active for periods smaller than the recombination time (typically $\sim 10^5$ years), with long gaps between “on” times (Chiang & Rappaport 1996). But, since it is not clear that either of these possible explanations should or does apply, it would be helpful to push the completeness limit for SSSs to lower X-ray luminosities. If the link between nebulae and SSSs can be established and if, as predicted (Rappaport et al. 1994, Di Stefano et al 1995), SSS nebulae can be distinguished from PNe by a careful examination of the full spectrum of excitation lines, then the nebulae may provide an independent guide to the size of SSS populations in external galaxies.

4.7. Relationship between SSSs and Supernova Remnants

The very soft X-ray emission of SSSs can resemble X-ray supernova remnants (SNRs). There are, e.g., two SSSs in M31 that were subsequently identified as SNRs based on extended morphology and multi-wavelength observations (Di Stefano et al. 2003, Kong et al. 2002b, 2003b). These two SNRs appear to be constant X-ray sources, which is consistent with the expected picture of SNRs. On the other hand, most of the SSSs in external galaxies are X-ray variables (Di Stefano & Kong 2003a; Kong & Di Stefano 2003). Although it is extremely difficult to study the morphology of X-ray sources at the distance of M104, and high resolution narrow-band optical imaging is not available, we can study the time variability of these X-ray sources to investigate their nature..

5. GC X-RAY SOURCES

5.1. Significance

Galactic GCs house approximately 100 times as many X-ray sources as would be expected based on their mass, suggesting that the efficiency of forming X-ray sources must be higher in GCs than elsewhere in the Galaxy (Clack 1975). A possible explanation is that the high stellar density near the cluster centers (as large as 10^6 stars pc^{-3}), can lead to stellar interactions in which close binaries containing white dwarfs (WDs) and neutron stars (NSs) can be formed. Eventually, either because dissipative processes (gravitational radiation or magnetic braking) bring the companion stars close enough for contact to be established, or else because the non-compact star begins to evolve and comes to fill its Roche lobe, mass transfer begins. Because the mass of the donor is generally limited by the turn off mass ($\sim 0.8M_{\odot}$), these systems are classified as low-mass X-ray binaries (LMXBs). Detailed calculations of interactions that form close binaries, follow the subsequent binary evolution, and include interactions which may occur after the close binaries are formed, show that a combination of 2-, 3-, and 4-body interactions can create X-ray binaries and lead them to be ejected to the outer parts of the cluster. (See, e.g., Phinney & Sigurdsson 1991.) It is considered likely that close binaries can be ejected from GCs, since the amount of energy needed to escape the cluster is a small fraction of the binary's binding energy.

LMXBs can also be formed in the field, because a subset of all primordial binaries are expected to evolve into close binaries in which a neutron star accretes mass from a low-mass companion. Before a primordial binary can turn on as an X-ray binary, several processes must occur. The formation of the neutron star occurs quickly, but the spiral in of the companion, or the companion's stellar evolution, can require several billion years. Because there are many uncertainties in the evolution of these systems and in the evolution of galaxy populations, it is difficult to accurately predict the numbers of LMXBs expected per unit mass, due to a single burst of early star formation. It has been suggested, however, that such systems may not be able to produce enough LMXBs to explain the numbers currently being discovered in early-type galaxies White, Sarazin, & Kulkarni(2002). (It is important to note that some of the early-type galaxies we observe may have had more complicated histories, with multiple epochs of star formation.) If not, then it is possible that the LMXBs we do see are systems that have been ejected from GCs. Indeed, testing this hypothesis has been an important motivator for study of the GC/LMXB connection. Meaningful tests must include the study of a set of

galaxies, including spirals, to search for evidence of differences in the LMXB/GC connection as exhibited by early- and late-type galaxies. Until now, M31 was the only spiral with bright enough GC X-ray sources to enable a comparison with the X-ray source population in distant ellipticals. M104 is therefore an important addition to the set of galaxies in which we can hope to study the LMXB/GC connection.

Below we focus our discussion on the GCs studied from the ground which have been matched with X-ray sources.

5.2. Optical Selection of Globular Clusters

Deep, wide-field images of M104 have been acquired with the CFHT12K mosaic camera at the Canada-France-Hawaii Telescope (CFHT) in order to investigate the optical characteristics of its large globular cluster system (GCS). A complete description of this photometry will appear in VanDalsen et al. (2003). In summary, the GCS exhibits a classically bimodal color distribution, with "blue" (metal-poor) and "red" (metal-rich) subpopulations centered at corresponding metallicities of $[\text{Fe}/\text{H}](\text{blue}) = -1.1$ and $[\text{Fe}/\text{H}](\text{red}) = -0.1$. The redder population – which makes up about one-third of the total GCS – is more centrally concentrated in spatial distribution than the bluer clusters.

In terms of the luminosity limit of our optical survey, our data reach nearly two magnitudes fainter than the normal "turnover" point (peak frequency) of the globular cluster luminosity function (GCLF). The GCLF turnover is at an absolute visual magnitude $M_V = -7.6$, corresponding to a cluster mass of $M \simeq 1.3 \times 10^5 M_{\odot}$, with little difference between the blue and red clusters. In short, the characteristics of the GCS strongly resemble those of the "standard" Milky Way GCS, simply scaled up to a total cluster population 7 or 8 times larger.

5.3. Properties of Matches

The procedure we have used to match GCs with X-ray sources is described in §3. We find 25 matches.

- Of these, 19 objects lie in the metal-rich side, while 6 objects lie in the metal-poor side, giving a 1:3 ratio of blue:red objects. However, a random sampling of globulars would globally yield a 2:1 ratio of blue:red objects, and approaching a 1:1 ratio of blue:red very close to M104. There also seems to be a lack of matches which are both bright and blue. We therefore find a result similar to others reported for NGC 4472 (Maccarone et al 2003, Kundu et al. 2002) and for the Milky Way and M31 (Bellazzini et al. 1995, but see also Di Stefano et al. 2002), that X-ray sources are preferentially found in GCs that are metal rich. (See Figure 6)
- Figure 7 illustrates the relationship between X-ray luminosity and the magnitude and color of the clusters housing X-ray sources. Two new features are worthy of note. First, the most luminous clusters in both *B* and *R* that have X-ray sources house only highly luminous X-ray sources ($L_X > 10^{38}$ erg s^{-1}). (In contrast, some clusters which are not as optically bright, house X-ray sources of lower luminosity, while others harbor bright X-ray sources.)
- Second, for X-ray sources with *L* greater than approximately 2.0×10^{38} erg s^{-1} , there is no obvious preference for GCs that are optically redder.
- None of the GC X-ray sources have luminosities greater than the Eddington limit for a $1.4M_{\odot}$ object Given the small numbers of sources at the highest luminosities, and the fact that transient behavior is common in LMXBs, this situation could

be different in future observations.

- Although the 4 brightest X-ray sources are not in GCs, GC X-ray sources dominate (in fact represent $\sim 68\%$ of all sources in the luminosity range $\sim 1.2-4 \times 10^{38} \text{ erg s}^{-1}$). That is, bright X-ray sources are most likely to be found in GC.

- As described in §4, one GC houses a soft X-ray source, X35, that could be an accreting BH with a mass of approximately $50M_{\odot}$.

5.4. Interpretation

The 4 brightest X-ray sources in M104 are super-Eddington for a $1.4M_{\odot}$ object; these 4 sources are not located in GCs. Nevertheless, the majority of (68%) all X-ray sources with $1.2 \times 10^{38} \text{ erg s}^{-1} < L_x < 4 \times 10^{38} \text{ erg s}^{-1}$ are in GCs. Were M104 located far enough from us, the majority of sources we observe could be in GCs. M104 provides a second example of a spiral galaxy (M31 being the first) in which the majority of the brightest sources are located in GCs.

Our data are consistent with previous findings that X-ray sources are found preferentially in red, hence metal-rich, GCs. An interesting twist, however, is that this preference for red GCs, is not expressed by the brightest X-ray sources. The least luminous GC X-ray sources in our sample do, on the other hand, have a strong preference for red GCs.

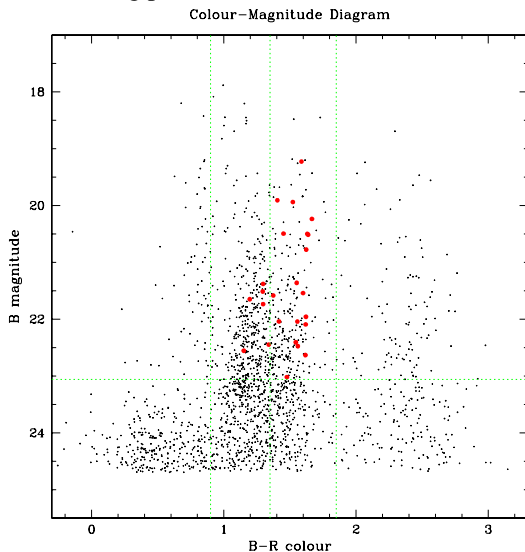


FIG. 6.— Color-magnitude diagram of all of the objects detected by the CFHT survey located within about 9 arcminutes (radius) of M104. This diagram shows globular clusters and non-cluster contaminants. The 25 X-ray matches are shown by large circles. The horizontal line (at $B = 23.06$) is the location of the GCLF turnover magnitude. The left and right vertical lines are the color limits used to identify GCs; they extend roughly $3-\sigma$ out from the GCS population, covering $(B-R)$ from 0.90–1.85. The middle vertical line represents the division between the blue (metal-poor) and red (metal-rich) populations, at $(B-R) = 1.35$.

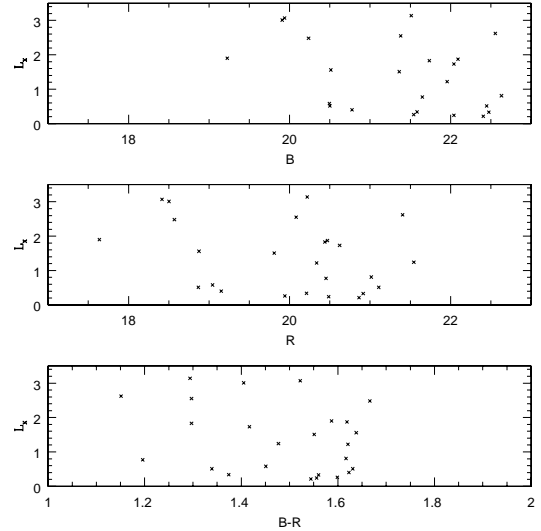


FIG. 7.— The X-ray luminosity, in units of $10^{38} \text{ erg s}^{-1}$, is plotted versus: B magnitude (top panel); R magnitude (middle panel); $B-R$ (bottom panel). Each point represent a single association between an X-ray source with X-ray luminosity L_x and an CFHT-detected GC with optical properties described by B , R , or $B-V$.

5.5. Models

Below we discuss possible explanations for the trends apparent in the data.

5.5.1. Thermal Time Scale Mass Transfer

The properties of the luminous X-ray source in the M31 GC Bo 375, suggested a new type of GC binary evolution model (Di Stefano et al. 2002). In this model, mass transfer is driven by the thermal time scale readjustment of the donor star to changes in the size of its Roche lobe. Mass transfer typically starts when the donor star has a mass that is within a few tenths of a solar mass of the NS, and is also slightly evolved (with core mass $\sim 0.1-0.25$). Because the donor is more massive than $0.8M_{\odot}$, this type of system can be found only in younger GCs and/or in GCs with such a high rate of stellar interactions that at least one NS can be expected to have a blue straggler donor. One proposed test of this model was to check if bright X-ray sources in the GCSs of external galaxies are likely to be found in young and/or optically bright GCs. This is exactly what we find in the Sombrero. Thus, although the model is not proved, M104 does provide some indirect evidence in its favor.

5.5.2. Multiplicity and Ejection

The correlation between optically bright GCs and high-luminosity X-ray sources is intriguing. It is likely that the large optical flux is indicative of a massive GC, in which stellar interactions producing X-ray binaries may be more frequent. More frequent interactions may lead to more X-ray sources per cluster. There are two possible checks for multiplicity.

Time Variability: GCs that do not house multiples, or that include only a small number ($\sim 2-3$) of individual components, could exhibit significant X-ray variability (by factors of 2–3) over the same time scales on which X-ray binaries are typically variable. Thus, over time scales of days, weeks, or months, we could expect to find evidence of variability. In contrast, GCs that have a high level of X-ray source multiplicity—i.e., in which

the total flux is a composite consisting of comparable contributions from more than a few sources—should be almost constant, since it is unlikely that many of the independent components will have L declining or increasing simultaneously.

Angular Resolvability: At the distance of M104, one arcsecond corresponds to roughly 43 pc, larger than the radii of typical GCs. Most of the GC X-ray sources in our sample are located away from the aim point, in regions where the angular resolution may be as large as several arcseconds. If, therefore, some of the high luminosity sources we detect in bright GCs are actually composites, one or more of the individual components may consist of X-ray sources that have been ejected from the cluster. It is possible that a subset of such systems could be resolved by pointed observations with *Chandra's* High Resolution Camera.

5.5.3. Giant Donors

The observations we have described introduce a puzzle: the brightest blue GCs do not host X-ray sources, while dimmer blue GCs can house X-ray sources that are among the brightest in the galaxy. We therefore seek to understand how they come to house extremely bright X-ray sources, while the brightest blue GCs do not appear to harbor X-ray sources, even X-ray sources that are ~ 10 times dimmer.

The thermal-time-scale scenario described above is likely to work in either young GCs, where the turn-off mass may be larger than $0.8M_{\odot}$, or in very massive GCs, in which the probability of a NS orbiting a blue straggler donor is larger. Similarly, multiplicity would seem to be most likely in large GCs with a high level of concentration and hence, high central surface brightness.

The problem posed above would seem to require another solution. Presumably the donor stars are old, and are less massive than their NS companions. In such cases, the mass transfer rate can be high if the donor is a giant. Such systems will exist in a GC only if a binary with total mass $\sim 2.2M_{\odot}$, and a separation of $\sim 50 - 1000R_{\odot}$ can survive. Some such binaries are considered “soft” in the GC environment, having less binding energy than the ambient kinetic energy of surrounding stars. Soft binaries have a good chance of being disrupted by a combination of distant interactions acting over time. Others of these binaries may not be formally “soft”, but, since they are likely to be found near the cluster center, where close interactions are most frequent; they can also be disrupted. Both mechanisms are least efficient at destroying the binaries with large separations in less massive and less highly concentrated GCs. It may therefore be that the most X-ray luminous X-ray sources in the less bright blue GCs are accreting NSs with giant donors.

It would be difficult to obtain direct evidence that a given GC X-ray source, even in M31, was an example of a NS accreting mass from a giant donor. A useful form of indirect evidence could, however, come from GCs in our own Galaxy. Specifically, we could attempt to establish the existence, in some clusters with low present-day interaction probabilities, of relatively luminous ($L > 10^{32}$ erg s $^{-1}$) CVs with giant donors. Galactic GCs are near enough that the optical properties of the X-ray binaries can be studied with *HST*, allowing general features of the model to be checked. WDs accreting from giant donors, which cannot presently be studied in external galaxies, may be more common analogs of the accreting NSs with giant donors. As such, they could provide insight into the environments that nurture such systems.

6. CONCLUSION AND PROSPECTS

M104 may be one of the richest theatres in which to study X-ray emission from galaxies. In this paper we have focused on the emission from non-nuclear point sources, since the diffuse emission (see Figure 2) which motivated this observation is the subject of a separate paper (Forman et al. 2003; see also Delain et al. 2001), as is the nuclear source (Pellegrini et al. 2003).

The primary science results we have extracted so far from the 18.5 ksec observation revolve around SSSs and the connection between GCs and LMXBs. We find SSSs inhabiting the bulge, disk and halo of M104. At least 4 of the halo sources are very soft, likely as soft as the SSSs known in the Magellanic Clouds. These are good candidates for nuclear-burning accreting WDs. The discovery of these sources several kiloparsecs from the disk, indicates that they are old systems, as should be expected for a subset of nuclear-burning WDs. In the halo as well as in the disk and bulge, we also find SSSs from which we have collected a small number of photons with energies above 1.1 keV. In some cases, photon statistics or the incomplete subtraction of background due to diffuse emission could be responsible for the harder photons. In most cases, however, the photons are likely to emanate from the system itself. Some SSSs exhibiting this harder emission may be supernova remnants. Since, however, similar sources have been discovered in other galaxies, including M31, M101, NGC 4472, M51, and M83, and since we have discovered that many such SSSs are variable on scales of months to years, it is likely that a large fraction are X-ray binaries. The harder photons from some SSS binaries may support a model in which the accretor is an intermediate-mass BH. We find a significant overdensity of SSSs within 1 kpc of the nucleus; future work will assess whether the overdensity is more pronounced for SSSs than for other X-ray sources. If it is, this could be indicative of tidal disruptions of giants by the $\sim 10^9M_{\odot}$ BH at the center of the Sombrero.

Regarding the LMXB/GC connection, we find that the fraction of bright X-ray sources in GCs is similar across galaxy types. We also find that those optically bright GCs that have X-ray sources house only bright X-ray sources. M104 provides another example of a galaxy in which X-ray sources are most likely to be found in red GCs; these clusters are presumably more metal rich and younger than bluer clusters. Interestingly enough, this preference for redder clusters does not seem to be expressed by the brightest ($L_X > 10^{38}$ erg s $^{-1}$) X-ray sources. Another interesting fact is that M104's optically brightest bluer clusters do not seem to house X-ray sources. We have sketched several models which can help to explain the trends seen in the data. Thermal-time-scale mass transfer can, in younger or more massive clusters, produce high luminosity systems. Multiplicity can play a role in some massive clusters. Accretion by a NS from a giant could be occurring in some blue clusters which house X-ray bright sources.

6.1. Prospects

An ultimate goal of X-ray observations of galaxies is to better understand the natures of the point sources and the processes by which stellar populations create them. To that end, the fact that M104 has a large X-ray source population, and is also well studied at other wavelengths, supports the process of relating X-ray sources to their environments. Its nearly edge-on orientation is also a boon, because it provides a rare opportunity to explore regions out of the disk of a spiral galaxy with a minimum of projection effects.

The Sombrero is not only an important galaxy to study in its own right, but it is also an important member of a set of external galaxies whose study will allow us to probe environmental effects on the creation, evolution, and properties of X-ray sources. Together with well-studied galaxies such as the Milky Way, M101, M83, and M81, it provides an example of an X-ray active spiral galaxy, supplementing information derived from the others because it is a bulge-dominated spiral and also because of its edge-on orientation. Consider the contrast with, e.g., M101, which is located at a comparable distance, but which is viewed nearly face-on. In M101 X-ray sources can be directly identified with disk stellar populations, but it is not possible to know which X-ray sources are actually located away from the galactic plane. The combination of studies of M101 and M104 can therefore play complementary roles. Another key difference is that the central region of M101 is not known to house a central BH, while M104 harbors a central BH with $10^9 M_{\odot}$. Already we know that the central concentration of X-ray sources in M101 is not as extreme as in M104, and that there are no bright SSSs with 1 kpc of the nucleus (Di Stefano & Kong 2003a, b). M31 does have a massive BH, but it is 30 times less massive than the Sombrero's; it will be important to compare the densities and properties of X-ray sources among

these galaxies. Because the Sombrero provides a link between disk-dominated and bulge-dominated galaxies, it will also be productive to compare the X-ray source population of M104 with those of elliptical galaxies, such as NGC 4472 (Kundu et al. 2002; Maccarone et al. 2003), NGC 4697 (Sarazin et al. 2001), and NGC 1399 (Angelini et al. 2001).

6.1.1. Future Observations

Future observations can not only provide a profile of the X-ray source distribution in the Sombrero, but can answer a range of science questions related to variability and to the environmental influences that affect the formation and evolution of X-ray sources in galaxies.

This work was supported by NASA under an LTSA grant, NAG5-10705. A.K.H.K. acknowledges support from the Croucher Foundation. W.E.H. is pleased to acknowledge financial support from the Natural Sciences and Engineering Research Council of Canada. R.D. would like to thank W. Forman and C. Jones for their careful reading of the paper and for comments, and R. Kraft and F.A. Primini for interesting conversations. We thank T.A. Russo for her careful reading of the manuscript.

REFERENCES

- Angelini, L., Loewenstein, M., & Mushotzky, R. F. 2001, *ApJ*, 557, L35
 Bellazzini, M., Pasquali, A., Federici, L., Ferraro, F. R., & Pecci, F. F. 1995, *ApJ*, 439, 687
 Brandt, W. N. et al. 2001, *AJ*, 122, 2810
 Chiang, E. & Rappaport, S. 1996, *ApJ*, 469, 255
 Cowley, A. P., Schmidtke, P. C., Crampton, D., & Hutchings, J. B. 1990, *ApJ*, 350, 288
 Crawford, D. F., Jauncey, D. L., & Murdoch, H. S. 1970, *ApJ*, 162, 405
 Cutri, R. M., et al. 2000, Explanatory Supplement to the 2MASS Second Incremental Data Release
 Davis, J.E. 2001, *ApJ*, 562, 575
 Delain, K. M., Forman, W. R., Jones, C., Murray, S. S., & Kraft, R. P. 2001, American Astronomical Society Meeting, 199, 1903
 Di Stefano, R., Paerels, F., & Rappaport, S. 1995, *ApJ*, 450, 705
 Di Stefano, R., & Rappaport, S. 1994, *ApJ*, 437, 733
 Di Stefano, R., Greiner, J., Murray, S., & Garcia, M. 2001, *ApJ*, 551, L37
 Di Stefano, R., Kong, A. K. H., Garcia, M. R., Barmby, P., Greiner, J., Murray, S. S., & Primini, F. A. 2002, *ApJ*, 570, 618
 Di Stefano, R., & Kong, A. K. H. 2003a, *ApJ*, in press (astro-ph/0301162)
 Di Stefano, R., & Kong, A. K. H. 2003b, *ApJ*, in preparation
 Fabbiano, G. & Juda, J.Z. 1997, *ApJ*, 476, 666
 Ford, H.C., Hui, X., Ciardullo, R., Jacoby, G.H., & Freeman, K.C. 1996, *ApJ*, 458, 455
 Forman, W. R. et al. 2003, in preparation.
 Friedman, R. B., Di Stefano, R., Kong, A. K. H., Barmby, P., & Kundu, A. 2002, American Astronomical Society Meeting, 201, 5414
 Freeman, P. E., Kashyap, V., Rosner, R., & Lamb, D. Q. 2002, *ApJS*, 138, 185
 Giacconi, R. et al. 2001, *ApJ*, 551, 624
 Greiner, J., Hasinger, G., & Kahabka, P. 1991, *A&A*, 246, L17
 Greiner, J., Tovmassian, G. H., Di Stefano, R., Prestwich, A., González-Riestra, R., Szentasko, L., & Chavarría, C. 1999, *A&A*, 343, 183
 Greiner, J. 2000, *New Astronomy*, 5, 137
 Greiner, J. & di Stefano, R. 1999, Highlights in x-ray astronomy : international symposium in honour of Joachim Trümper's 65th birthday, June 17-19, 1998, Garching, Germany : symposium proceedings / edited by Bernd Aschenbach Michael J. Freyberg. Garching : Max-Planck-Institut für extraterrestrische Physik, 1999. (MPE report, No. 272, ISSN 0178-0719), p.66, 66
- Harris, D. E., et al. 1993, The Einstein Observatory Catalog of IPC X-Ray Sources. Volume 1E: Documentation (NASA TM-108401), 121
 Kong, A. K. H., Garcia, M. R., Primini, F. A., Murray, S. S., Di Stefano, R., & McClintock, J. 2002a, *ApJ*, 577, 738
 Kong, A. K. H., Garcia, M. R., Primini, F. A., & Murray, S. S. 2002b, *ApJ*, 580, L125
 Kong, A. K. H. & Di Stefano, R. 2003, *ApJ*, 590, L13
 Kong, A.K.H., Di Stefano, R., Garcia, M.R., & Greiner, J. 2003a, *ApJ*, 585, 298
 Kong, A.K.H., Sjouwerman, L.O., Williams, B.F., Garcia, M.R., & Dickel, J.R. 2003b, *ApJ*, 590, L21
 Kundu, A., Maccarone, T. J., & Zepf, S. E. 2002, *ApJ*, 574, L5
 Kylafis, N. D. & Xilouris, E. M. 1993, *A&A*, 278, L43
 Larsen, S.S., Forbes, D.A., & Brodie, J.P. 2001, *MNRAS*, 327, 1116
 Long, K. S., Helfand, D. J., & Grabelsky, D. A. 1981, *ApJ*, 248, 925
 Maccarone, T. J., Kundu, A., & Zepf, S. E. 2003, *ApJ*, 586, 814
 Monet D.G, et al. 2003, The USNO-B1.0 Catalog
 Pellegrini, S., Baldi, A., Fabbiano, G., & Kim, D.-W. 2003, *ApJ*, submitted
 Pellegrini, S., Fabbiano, G., Fiore, F., Trinchieri, G., & Antonelli, A. 2002, *A&A*, 383, 1
 Pellegrini, S., Venturi, T., Comastri, A., Fabbiano, G., Fiore, F., Vignali, C., Morganti, R., & Trinchieri, G. 2003, *ApJ*, 585, 677
 Phinney, E. S. & Sigurdsson, S. 1991, *Nature*, 349, 220
 Rappaport, S., Chiang, E., Kallman, T., & Malina, R. 1994, *ApJ*, 431, 237
 Remillard, R. A., Rappaport, S., & Macri, L. M. 1995, *ApJ*, 439, 646
 Sarazin, C.L., Irwin, J.A., & Bregman, J.N. 2001, *ApJ*, 556, 533
 Swartz, D. A., Ghosh, K. K., Suleimanov, V., Tennant, A. F., & Wu, K. 2002, *ApJ*, 574, 382
 Vandalfsen, M., Kavelaars, J. J., Harris, W. E., Hanes, D., & Harris, G. 2001, Bulletin d'information du telescope Canada-France-Hawaii, 43, 10
 van den Heuvel, E.P.J., Bhattacharya, D., Nomoto, K., & Rappaport, S.A. 1992, *A&A*, 262, 97
 Wang, Q. 1991, *MNRAS*, 252, 47P
 White, R. E., Sarazin, C. L., & Kulkarni, S. R. 2002, *ApJ*, 571, L23

TABLE 1
SOURCE LIST

Object	R.A. (h:m:s)	Dec. (°:':")	Soft	Net Counts Medium	Hard	L_X^a ($\times 10^{38}$)	Optical Magnitude	Note
X1	12:39:38.7	-11:38:51.1	21.7 ± 4.8	11.1 ± 3.4	-0.5 ± 0.2	0.69	$B = 13.8, R = 12.5, K = 10.9$	star, SSS-med
X2	12:39:42.3	-11:36:56.1	7.6 ± 2.8	9.4 ± 3.0	6.9 ± 2.6	0.73		
X3	12:39:43.1	-11:36:44.2	2.9 ± 1.8	6.0 ± 2.5	6.7 ± 2.7	0.48		
X4	12:39:44.2	-11:36:00.5	30.3 ± 5.6	21.4 ± 4.6	7.2 ± 2.8	1.76		
X5	12:39:45.2	-11:38:49.5	630.2 ± 25.1	144.9 ± 12.0	28.8 ± 5.3	19.20	$B = 10.3, R = 9.7, K = 8.4$	star, SSS- σ
X6	12:39:45.2	-11:36:00.4	36.6 ± 6.1	39.5 ± 6.3	25.0 ± 5.1	2.48	$B = 20.0, R = 18.5, K = 15.6$	CFHT
X7	12:39:45.6	-11:39:33.1	7.2 ± 2.6	4.9 ± 2.2	10.0 ± 3.1	0.67	$B = 19.9, R = 18.9$	star
X8	12:39:47.2	-11:38:14.6	9.3 ± 3.0	6.3 ± 2.5	4.9 ± 2.3	0.63		
X9	12:39:48.6	-11:37:13.0	87.5 ± 9.3	64.3 ± 8.0	24.2 ± 4.9	5.42		
X10	12:39:50.1	-11:37:41.7	2.8 ± 1.8	3.1 ± 1.8	1.8 ± 1.4	0.24		
X11	12:39:50.5	-11:39:14.5	19.1 ± 4.4	19.5 ± 4.4	13.2 ± 3.6	1.56	$B = 20.2, R = 19.0$	star
X12	12:39:50.9	-11:38:23.3	31.5 ± 5.6	44.4 ± 6.6	27.9 ± 5.3	3.14		CFHT
X13	12:39:51.1	-11:36:47.7	7.6 ± 2.9	9.3 ± 3.0	3.0 ± 1.7	0.59		
X14	12:39:51.1	-11:39:28.4	-0.6 ± 0.2	3.9 ± 2.0	4.9 ± 2.2	0.26		
X15	12:39:51.1	-11:38:33.7	9.3 ± 3.0	5.2 ± 2.2	1.6 ± 1.4	0.40		SSS- 3σ 1
X16	12:39:51.9	-11:35:51.9	38.2 ± 6.2	27.5 ± 5.3	8.8 ± 2.9	2.29		CFHT
X17	12:39:53.4	-11:37:09.3	6.1 ± 2.7	8.0 ± 2.8	4.1 ± 2.0	0.57		
X18	12:39:54.0	-11:38:25.1	30.7 ± 5.5	3.0 ± 1.7	0.8 ± 1.0	0.84		SSS- 3σ
X19	12:39:54.1	-11:37:13.0	4.5 ± 2.3	4.0 ± 2.0	2.0 ± 1.4	0.33		
X20	12:39:54.6	-11:36:02.5	5.3 ± 2.4	1.0 ± 1.0	2.0 ± 1.5	0.26		CFHT
X21	12:39:54.8	-11:37:30.3	1.5 ± 1.4	6.1 ± 2.5	1.0 ± 1.0	0.21		SSS-med
X22	12:39:54.9	-11:37:08.6	6.0 ± 2.7	7.9 ± 2.9	11.4 ± 3.3	0.78		
X23	12:39:55.1	-11:37:37.0	0.6 ± 1.0	11.3 ± 3.3	20.5 ± 4.5	1.01		
X24	12:39:55.4	-11:38:48.9	17.2 ± 4.1	10.3 ± 3.2	11.8 ± 3.4	1.22		CFHT
X25	12:39:55.5	-11:37:32.1	4.7 ± 2.2	3.9 ± 2.0	1.9 ± 1.4	0.32		
X26	12:39:55.8	-11:34:48.1	19.4 ± 4.5	16.3 ± 4.0	14.9 ± 3.9	1.56	$B = 19.3, R = 18.4$	CFHT
X27	12:39:55.8	-11:37:31.4	3.2 ± 2.0	7.2 ± 2.7	3.9 ± 2.0	0.42		
X28	12:39:55.9	-11:37:42.1	1.5 ± 1.4	3.9 ± 2.0	4.9 ± 2.2	0.32		
X29	12:39:56.4	-11:31:54.2	32.6 ± 5.9	40.3 ± 6.3	32.5 ± 5.9	3.07	$B = 19.7, R = 18.3, K = 15.6$	CFHT
X30	12:39:56.4	-11:37:59.0	17.2 ± 4.1	10.3 ± 3.2	6.0 ± 2.4	1.03		
X31	12:39:56.4	-11:37:24.3	13.9 ± 4.1	11.4 ± 3.4	6.1 ± 2.4	0.99		
X32	12:39:56.5	-11:38:30.5	7.9 ± 2.8	5.1 ± 2.2	10.0 ± 3.1	0.68		
X33	12:39:56.9	-11:36:58.6	3.7 ± 2.0	3.9 ± 2.0	8.1 ± 2.8	0.42		
X34	12:39:57.2	-11:37:03.9	5.9 ± 2.5	1.9 ± 1.4	2.6 ± 1.7	0.32		
X35	12:39:57.2	-11:36:33.6	4.5 ± 2.2	3.1 ± 1.7	0.8 ± 1.0	0.21		CFHT, SSS-noh
X36	12:39:57.3	-11:36:29.5	5.8 ± 2.5	2.9 ± 1.7	-0.2 ± 0.1	0.19		SSS-noh
X37	12:39:57.3	-11:37:50.3	6.1 ± 2.5	3.1 ± 1.7	0.0 ± 0.0	0.23		SSS-med
X38	12:39:57.4	-11:37:19.8	51.1 ± 7.1	43.9 ± 6.6	46.4 ± 6.8	4.17		
X39	12:39:57.4	-11:37:52.8	14.4 ± 3.8	12.4 ± 3.5	7.9 ± 2.8	1.07		
X40	12:39:57.4	-11:37:33.6	5.8 ± 2.5	3.0 ± 1.7	5.8 ± 2.5	0.46		
X41	12:39:57.7	-11:38:52.9	11.9 ± 3.5	11.2 ± 3.3	6.9 ± 2.6	0.93		
X42	12:39:57.7	-11:37:14.6	6.9 ± 2.7	3.9 ± 2.0	2.0 ± 1.4	0.40		
X43	12:39:57.9	-11:37:02.3	15.9 ± 4.0	12.2 ± 3.5	3.0 ± 1.7	0.96		
X44	12:39:57.9	-11:37:34.5	9.0 ± 3.0	15.4 ± 3.9	4.8 ± 2.2	0.87		
X45	12:39:58.3	-11:37:17.8	18.3 ± 4.3	10.3 ± 3.2	7.0 ± 2.6	1.06		
X46	12:39:58.5	-11:37:21.2	12.1 ± 3.5	3.9 ± 2.0	6.1 ± 2.4	0.68		
X47	12:39:58.6	-11:37:27.6	7.0 ± 2.7	8.4 ± 2.9	8.0 ± 2.8	0.72		<i>HST</i>
X48	12:39:58.7	-11:38:20.6	8.3 ± 2.9	2.1 ± 1.4	-0.1 ± 0.0	0.23		SSS-noh
X49	12:39:58.7	-11:37:21.4	8.1 ± 2.8	7.2 ± 2.7	3.8 ± 2.0	0.59		
X50	12:39:58.8	-11:37:24.9	27.6 ± 5.3	13.6 ± 3.6	11.3 ± 3.3	1.59		<i>HST</i>
X51	12:39:58.8	-11:37:00.2	3.7 ± 2.0	5.0 ± 2.2	2.6 ± 1.7	0.35		
X52	12:39:58.9	-11:36:54.6	9.8 ± 3.2	9.3 ± 3.0	6.9 ± 2.6	0.81		CFHT
X53	12:39:58.9	-11:38:37.9	10.8 ± 3.3	21.4 ± 4.6	8.0 ± 2.8	1.24		CFHT, <i>HST</i>
X54	12:39:59.0	-11:35:12.0	24.0 ± 4.9	40.2 ± 6.3	22.08 ± 4.7	2.62		CFHT
X55	12:39:59.1	-11:37:19.4	61.0 ± 7.8	28.9 ± 5.4	10.3 ± 3.2	2.93		<i>HST</i>
X56	12:39:59.3	-11:38:28.1	18.3 ± 4.2	20.3 ± 4.5	10.5 ± 3.2	1.51		CFHT, <i>HST</i>
X57	12:39:59.3	-11:36:50.0	8.7 ± 3.0	1.8 ± 1.4	-0.3 ± 0.1	0.25		SSS-med

TABLE 1—Continued

Object	R.A. (h:m:s)	Dec. (°:':")	Soft	Net Counts Medium	Hard	L_X^a ($\times 10^{38}$)	Optical Magnitude	Note
X58	12:39:59.3	-11:38:46.0	1.8 ± 1.4	3.0 ± 1.7	2.9 ± 1.7	0.24		CFHT, <i>HST</i>
X59	12:39:59.4	-11:37:26.8	57.4 ± 7.5	39.7 ± 6.3	25.5 ± 5.0	3.78		<i>HST</i>
X60	12:39:59.4	-11:37:22.7	709.4 ± 26.6	999.9 ± 31.6	906.5 ± 30.1	80.32		Nucleus
X61	12:39:59.5	-11:37:01.8	22.4 ± 4.7	16.4 ± 4.0	19.5 ± 4.4	1.80		
X62	12:39:59.6	-11:37:29.0	8.7 ± 3.0	6.2 ± 2.5	-0.3 ± 0.1	0.37		SSS-med
X63	12:39:59.7	-11:35:24.8	18.9 ± 4.3	21.2 ± 4.6	19.1 ± 4.3	1.73		CFHT
X64	12:39:59.8	-11:37:16.1	41.3 ± 6.4	10.1 ± 3.2	1.8 ± 1.4	1.33		SSS-HR1
X65	12:39:59.8	-11:34:54.4	10.7 ± 3.3	8.0 ± 2.8	6.2 ± 2.6	0.77		CFHT
X66	12:39:59.8	-11:37:00.2	7.9 ± 2.8	9.2 ± 3.0	4.1 ± 2.0	0.66		
X67	12:39:59.9	-11:36:22.8	36.7 ± 6.1	37.2 ± 6.1	22.4 ± 4.7	2.89		
X68	12:39:59.9	-11:37:39.7	2.7 ± 1.7	2.0 ± 1.4	3.0 ± 1.7	0.24		
X69	12:40:00.0	-11:37:26.6	11.2 ± 3.3	11.4 ± 3.3	7.0 ± 2.6	0.91		
X70	12:40:00.0	-11:37:08.5	28.7 ± 5.3	35.0 ± 5.9	19.5 ± 4.4	2.56		
X71	12:40:00.1	-11:35:42.0	13.8 ± 3.7	-0.0 ± 0.0	0.0 ± 0.0	0.14		SSS-HR
X72	12:40:00.2	-11:37:22.6	19.7 ± 4.4	20.8 ± 4.5	13.2 ± 3.6	1.59		
X73	12:40:00.3	-11:37:23.2	54.0 ± 7.3	29.1 ± 5.4	19.4 ± 4.4	3.06		<i>HST</i>
X74	12:40:00.4	-11:37:17.6	7.8 ± 2.8	8.1 ± 2.8	1.7 ± 1.4	0.55		
X75	12:40:00.7	-11:37:12.5	8.1 ± 2.8	8.1 ± 2.8	0.7 ± 1.0	0.42		SSS-med
X76	12:40:00.7	-11:35:19.4	31.8 ± 5.6	27.1 ± 5.2	25.1 ± 5.0	2.55		CFHT
X77	12:40:00.7	-11:37:04.3	13.2 ± 3.6	12.3 ± 3.5	15.4 ± 3.9	1.26		
X78	12:40:00.7	-11:37:30.3	3.5 ± 2.0	5.2 ± 2.2	2.9 ± 1.7	0.36		
X79	12:40:00.9	-11:36:53.9	138.3 ± 11.7	111.7 ± 10.5	42.2 ± 6.5	8.87		
X80	12:40:01.0	-11:37:08.3	6.5 ± 2.7	7.1 ± 2.6	5.1 ± 2.2	0.58		CFHT
X81	12:40:01.0	-11:37:00.9	15.0 ± 3.9	2.5 ± 1.7	7.0 ± 2.6	0.69		<i>HST</i>
X82	12:40:01.1	-11:37:23.8	391.3 ± 19.7	81.8 ± 9.0	5.9 ± 2.4	11.48		SSS- σ
X83	12:40:01.3	-11:37:02.0	3.9 ± 2.0	6.1 ± 2.4	2.7 ± 1.7	0.39		
X84	12:40:01.3	-11:37:29.8	9.1 ± 3.0	10.4 ± 3.2	16.4 ± 4.0	1.08		
X85	12:40:01.4	-11:40:10.1	2.7 ± 1.7	3.8 ± 2.0	1.9 ± 1.4	0.26		
X86	12:40:02.0	-11:39:40.1	71.5 ± 8.4	0.0 ± 0.0	-0.1 ± 0.1	1.55		SSS-HR
X87	12:40:02.0	-11:37:07.1	6.6 ± 2.6	7.1 ± 2.6	2.8 ± 1.7	0.51		CFHT, <i>HST</i>
X88	12:40:02.0	-11:38:46.4	5.1 ± 2.3	1.9 ± 1.4	1.8 ± 1.4	0.28		
X89	12:40:02.2	-11:37:53.8	19.6 ± 4.4	3.9 ± 2.0	10.2 ± 3.2	1.04		
X90	12:40:02.2	-11:37:18.6	14.9 ± 3.9	8.9 ± 3.0	13.1 ± 3.6	1.08		
X91	12:40:02.2	-11:38:01.5	6.7 ± 2.7	3.7 ± 2.0	6.1 ± 2.4	0.51		CFHT, <i>HST</i>
X92	12:40:02.3	-11:37:11.7	8.7 ± 3.0	6.2 ± 2.4	1.0 ± 1.0	0.40		SSS-med
X93	12:40:02.4	-11:38:52.3	10.0 ± 3.2	1.9 ± 1.4	3.9 ± 2.0	0.49		
X94	12:40:02.8	-11:37:16.8	11.9 ± 3.5	6.1 ± 2.4	6.0 ± 2.4	0.74		
X95	12:40:03.1	-11:40:04.9	4.8 ± 2.2	6.1 ± 2.4	6.9 ± 2.6	0.55	$B = 18.0, R = 16.5, K = 14.6$	star
X96	12:40:03.6	-11:37:39.2	3.7 ± 2.0	7.9 ± 2.9	11.2 ± 3.3	0.70		
X97	12:40:03.7	-11:32:43.0	13.4 ± 3.9	11.0 ± 3.3	13.5 ± 4.0	1.10	$B = 20.7, R = 19.6$	star
X98	12:40:03.7	-11:37:00.9	7.4 ± 2.8	3.0 ± 1.7	0.8 ± 1.0	0.28		SSS-med
X99	12:40:04.5	-11:36:37.5	13.9 ± 3.7	7.4 ± 2.7	6.0 ± 2.5	0.84		
X100	12:40:04.6	-11:37:35.8	2.5 ± 1.7	9.1 ± 3.0	14.3 ± 3.7	0.81		
X101	12:40:04.7	-11:38:28.8	1.2 ± 1.4	4.0 ± 2.0	5.1 ± 2.2	0.33		CFHT, <i>HST</i>
X102	12:40:04.8	-11:37:21.0	15.4 ± 4.0	2.7 ± 1.7	1.8 ± 1.4	0.48		SSS- 3σ
X103	12:40:05.0	-11:37:32.3	9.0 ± 3.0	8.3 ± 2.8	13.3 ± 3.6	0.91		
X104	12:40:05.3	-11:35:00.0	18.0 ± 4.3	24.2 ± 4.9	17.1 ± 4.3	1.83		CFHT
X105	12:40:05.5	-11:39:40.5	23.0 ± 4.8	1.7 ± 1.4	4.7 ± 2.2	0.82		
X106	12:40:05.7	-11:37:11.2	20.0 ± 4.5	14.3 ± 3.8	8.9 ± 3.0	1.30		<i>HST</i>
X107	12:40:06.9	-11:37:22.0	4.4 ± 2.2	3.1 ± 1.7	1.8 ± 1.4	0.30		
X108	12:40:07.0	-11:37:53.2	20.4 ± 4.5	18.7 ± 4.3	21.4 ± 4.6	1.87		CFHT, <i>HST</i>
X109	12:40:08.2	-11:34:46.2	3.9 ± 2.3	9.4 ± 3.1	0.8 ± 1.5	0.36		SSS-med
X110	12:40:08.4	-11:37:11.3	10.0 ± 3.2	3.0 ± 1.7	1.8 ± 1.4	0.35		SSS-HR1
X111	12:40:08.9	-11:38:17.2	11.4 ± 3.4	1.9 ± 1.4	0.0 ± 0.0	0.30		SSS- 3σ
X112	12:40:09.5	-11:36:46.6	21.5 ± 4.6	12.3 ± 3.5	10.1 ± 3.2	1.32		
X113	12:40:09.7	-11:36:44.7	2.9 ± 1.7	5.1 ± 2.2	2.9 ± 1.7	0.34		CFHT
X114	12:40:10.4	-11:36:38.7	41.4 ± 6.5	33.0 ± 5.7	26.5 ± 5.1	3.01		CFHT

TABLE 1—*Continued*

Object	R.A. (h:m:s)	Dec. (°:′:″)	Soft	Net Counts Medium	Hard	L_X^a ($\times 10^{38}$)	Optical Magnitude	Note
X115	12:40:10.8	-11:32:58.1	22.2 ± 4.9	18.3 ± 4.3	23.4 ± 4.9	1.90	$B = 19.3, R = 17.6, K = 14.8$	CFHT
X116	12:40:11.4	-11:34:42.9	8.2 ± 3.2	8.2 ± 3.0	12.5 ± 3.7	0.89		
X117	12:40:12.3	-11:40:05.3	6.2 ± 2.7	7.0 ± 2.7	7.5 ± 2.9	0.63		
X118	12:40:12.7	-11:36:30.9	3.9 ± 2.3	3.8 ± 2.0	4.1 ± 2.3	0.37		
X119	12:40:12.9	-11:39:03.0	9.0 ± 3.2	2.8 ± 1.7	3.8 ± 2.0	0.51		
X120	12:40:13.7	-11:37:52.2	13.4 ± 3.8	6.8 ± 2.7	2.6 ± 1.7	0.62		
X121	12:40:15.2	-11:33:07.6	21.3 ± 5.4	50.1 ± 7.2	15.2 ± 4.4	2.63		3 USNO stars
X122	12:40:15.5	-11:37:34.8	6.1 ± 2.6	5.5 ± 2.4	4.8 ± 2.4	0.48		

Note. — The columns give the source number, the position (J2000.0), the net counts in the three energy bands (soft: 0.1–1.1 keV; medium: 1.1–2 keV; hard: 2–7 keV), the 0.3–7 keV luminosity. The conversion to luminosities assumes an absorbed power-law spectrum with a photon index of 2 and $N_H = 5 \times 10^{20} \text{ cm}^{-2}$. For SSSs, we assume a blackbody model with $kT=125 \text{ eV}$ and $N_H = 5 \times 10^{20} \text{ cm}^{-2}$. The B and R magnitudes are taken from USNO-B1.0 catalog, while the K magnitude is from the 2MASS catalog. CFHT: Globular clusters from the ground; *HST*: Globulars clusters from *HST*; SSS-HR, SSS-HR1, SSS- 3σ , SSS- $3\sigma 1$, SSS- σ , SSS-med, SSS-noh: SSS category from Di Stefano and Kong (2003b).

^aLuminosity in 0.3–7 keV (erg s^{-1}), assuming $d = 8.9 \text{ Mpc}$, and a power-law model with $N_H = 5 \times 10^{20} \text{ cm}^{-2}$, and $\alpha = 2$ for all sources except SSSs for which a blackbody model with $N_H = 5 \times 10^{20} \text{ cm}^{-2}$, and $kT = 125 \text{ eV}$ is applied.

TABLE 2
SPECTRAL FITS TO THE BRIGHTEST X-RAY SOURCES IN M 104

Object	N_H (10^{20} cm^{-2})	α	kT/kT_{RS} (keV)	χ^2_{ν}/dof	L_X^a
X5	11.1^{+10}_{-6}	$2.86^{+0.68}_{-0.57}$	$0.36^{+0.05b}_{-0.06}$	1.64/25	26.5^c
X9	$6.1^{+7.6}_{-6.0}$	$2.0^{+0.45}_{-0.47}$		0.8/5	6.34
X38	$2.1^{+8.4}_{-2.1}$	$1.13^{+0.39}_{-0.32}$		0.85/10	5.89
X59	$5.1^{+10}_{-5.1}$	$1.78^{+0.33}_{-0.53}$		0.88/8	4.27
X79	$10.8^{+6.6}_{-6.7}$	$2.04^{+0.43}_{-0.28}$		0.83/10	12
X82	$0.9^{+4.6}_{-0.9}$		$0.18^{+0.02}_{-0.02}$	0.71/15	8.9

Note. — All quoted uncertainties are at the 90% confidence level.

^a Unabsorbed luminosity ($\times 10^{38} \text{ erg s}^{-1}$) in 0.3–7 keV, assuming a distance of 8.9 Mpc.

^b Raymond-Smith temperature.

^c X5 is a foreground star. If assuming a distance of 4kpc, the 0.3–7 keV luminosity is $5.36 \times 10^{32} \text{ erg s}^{-1}$.